



SHocks: structure, AcceleRation, dissiPation

Work Package 2
Structure of heliospheric shocks

Deliverable D2.4
Technical report on high-Mach number shock
characteristics

Prepared by: Michael Gedalin
on behalf of SHARP

This project has received funding from the European Union's Horizon 2020
research and innovation programme under grant agreement No 101004131



Document Change Record

Issue	Date	Author	Details
1.0	14.06.23	M. Gedalin	send to other co-authors for comments
1.1	26.06.23	M. Gedalin	final version

Table of Contents

1	Summary	3
2	Introduction	3
3	Results	4
3.1	Non-specularly reflected ions and foot formation	4
3.2	Role of overshoot	4
3.3	Stabilizing effect of the reflected-transmitted ions	6
3.4	Relation of the ion distributions to the shock structure	7
3.5	An analytical model of rippling and implications	8
3.6	Ion dynamics in non-rippled vs rippled shocks	8
3.7	Nonlocal reflection	11
4	References	12

1 Summary

A collisionless shock is a self-regulatory structure. The main condition of a collisionless shock sustainability is that a fast and stable transfer of the mass, momentum, and energy are transferred from upstream to downstream. By "fast" we mean that the transition occurs at scales substantially small than the typical MHD scales. By "stable" we mean that there are no major disruptions of the particle, momentum, and energy fluxes, except those caused by the changes of the ambient conditions. With the increase of the Mach number, the shock structure evolves to ensure that the fluxes are constant with proper spatial and temporal averaging. The fluxes are carried mainly by ions, so that there is an intimate two-way relation of the ion motion and distributions and the shock structure. In this way, with the increase of the Mach number a strong shock overshoot develops, followed by an undershoot and possibly more magnetic oscillations. At even higher Mach number shocks become rippled, and subsequently probably reforming and turbulent. The last two stages were beyond the scope of the present study. In the ramp-overshoot and rippled shocks ion reflection plays the most important role. Therefore, studies of the structure of high Mach number shocks cannot be separated from studies of ion reflection. We have shown that ion reflection is non-specular and their turning distances are smaller than it was thought (Balikhin & Gedalin, 2022). We elucidated the role of the overshoot in ion reflection (Gedalin et al., 2023a) and the stabilizing effect of the reflected ions (Gedalin & Sharma, 2023; Sharma & Gedalin, 2023, submitted). We established the relation of the non-gyrotropic (Gedalin, 2022) and gyrotropic-anisotropic (Gedalin et al., 2022) ion distributions to the shock structure. We proposed a model of the shock rippling and analyzed implications for waves and particle distributions (Gedalin & Ganushkina, 2022). Non-locality of ion reflection has been analyzed in detail and was proposed as a mechanism of rippling onset (Gedalin, 2023, submitted). Ion dynamics in high-Mach number shocks was studied numerically (Gedalin et al., 2023b, accepted) and observationally (Dimmock et al., 2023, submitted), while comparing planar and rippled shock models.

2 Introduction

A collisionless shock is a self-regulatory structure. The main condition of a collisionless shock sustainability is that a fast and stable transfer of the mass, momentum, and energy are transferred from upstream to downstream. By "fast" we mean that the transition occurs at scales substantially small than the typical MHD scales. By "stable" we mean that there are no major disruptions of the particle, momentum, and energy fluxes, except those caused by the changes of the ambient conditions. With the increase of the Mach number, the shock structure evolves to ensure that the fluxes are constant with proper spatial and temporal averaging. The fluxes are carried mainly by ions, so that there is an intimate two-way relation of the ion motion and distributions and the shock structure. Low-Mach number shocks have at most weak overshoots and otherwise a monotonic magnetic field increase across the shock transition. Directly transmitted ions are capable of ensuring constant fluxes throughout a planar stationary structure. The magnetic overshoot is produced due to the deceleration of the directly transmitted ions and

the necessity to balance the decrease of the plasma pressure by the corresponding increase of the magnetic pressure. With the increase of the Mach number the overshoot becomes larger and starts reflecting ions. The ion reflection is essentially non-specular, produced by the electrostatic and magnetic forces together. For quasi-perpendicular shocks most or almost all reflected ions gyrate in the upstream, producing a foot, and return back to the shock to cross it again and form the population of reflected-transmitted ions. These ions have substantially higher gyration velocities than the directly transmitted ions, thus contributing significantly to the downstream ion pressure even if their density is low. Too strong or too weak reflection would cause pressure imbalance and disrupt the shock. As long as the ramp-overshoot structure is capable of ensuring of just the right amount of reflected ions, the shock can remain nearly planar and stationary. Once this is not longer possible, a shock must develop a new structure, which would remain stable, at least on average. Apparently, this happens via development a rippled time-dependent shock front. Understanding physics of high-Mach number shocks requires understanding the ion motion and distributions in the ramp-overshoot and in the rippled structures, and the influence of these ion distributions on the field profile.

3 Results

This is the most ambitious and effort consuming part of the study. Understanding the structure of high-Mach number shocks is like combining parts of a puzzle in one complete picture, while these puzzles have to be identified and solved. Below is the description of the parts of the whole.

3.1 Non-specularly reflected ions and foot formation

Ions are reflected by the combined effect of the electrostatic cross-shock field and the increasing magnetic field in the ramp and overshoot. Upon being reflected they gyrate ahead of the ramp and form a foot. The foot length is closely related to the turning distance of these ions. Figure 1 shows histograms of the turning distances of reflected ions in the foot for $\theta_{Bn} = 70^\circ$, $\beta = 0.3$, and for three values of the cross-shock potential $s = 0.4, 0.5, 0.6$. The efficiency of reflection and the turning distance decrease rapidly with the decrease of the potential. The widely used expression (Gosling & Thomsen, 1985) overestimates the foot length by a factor of two.

3.2 Role of overshoot

The pressure balance reads

$$p_{xx} + \frac{B^2}{2M^2} = \text{const} \quad (1)$$

where $p_{xx} = m \int v_x^2 f(\mathbf{v}) d^3\mathbf{v}$ is normalized on the upstream dynamic pressure $n_u m V_u^2$ and the magnetic field is normalized on the upstream magnetic field B_u . The downstream pressure of the directly transmitted ions is determined by the deceleration and later gyration. Since the cross-shock potential scales as M^2 , the

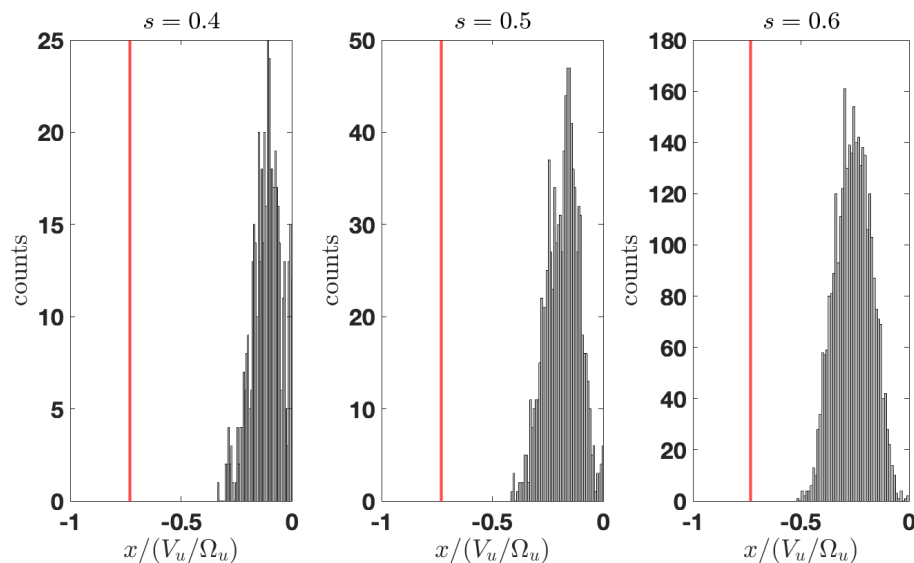


Figure 1: Histograms of the turning distances of the reflected ions in the foot for $\theta_{Bn} = 70^\circ$, $\beta = 0.3$, and three values of the cross-shock potential $s = 0.4, 0.5, 0.6$. The red line marks the position of the upstream edge of the foot according to Gosling & Thomsen (1985).

deceleration does not depend directly on the Mach number. The gyration depends on the downstream magnetic field which is limited the classical Rankine-Hugoniot relations at $B = 4$. Yet, the pressure balance requires that the downstream magnetic field scale as M^2 . Thus, at sufficiently high Mach numbers the directly transmitted ions alone cannot ensure pressure balance. Reflected-transmitted ions significantly increase the downstream p_{xx} and thus cannot restore the pressure balance. Overshoot enhances ion reflection, as shown in Figure 2.

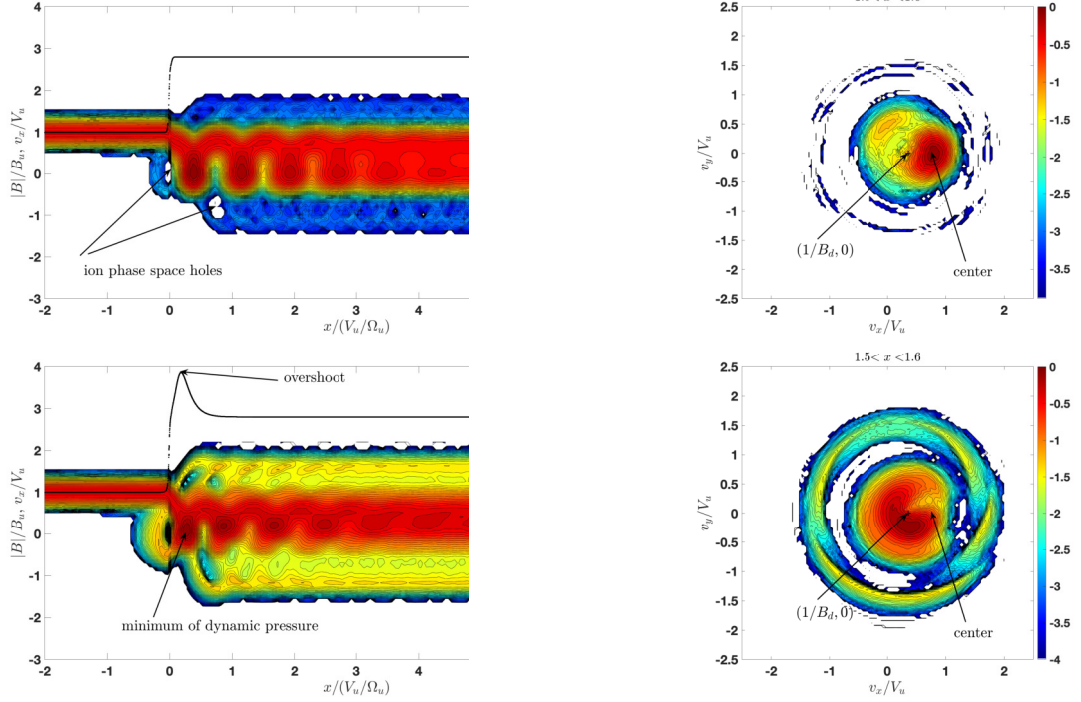


Figure 2: Top left: reduced 1D distribution $f(x, v_x)$, together with the magnetic profile, no overshoot. Top right: 2D reduced distribution $f(v_x, v_y)$ integrated over the slab $1.5 < x < 1.6$, no overshoot. Bottom left: reduced 1D distribution $f(x, v_x)$, together with the magnetic profile, with overshoot. Bottom right: 2D reduced distribution $f(v_x, v_y)$ integrated over the slab $1.5 < x < 1.6$, with overshoot.

Thus, the main effect is ion reflection which is absent or too weak without an overshoot. Without reflected ions the downstream distribution is under-heated, non-gyrotropy relaxation is slow, and eventual anisotropy is very strong. An overshoot enhances ion reflection and, therefore, ion heating.

3.3 Stabilizing effect of the reflected-transmitted ions

Using numerical tracing (Gedalin & Sharma, 2023, submitted) and analytical approach (Sharma & Gedalin, 2023, submitted), we have shown that the reflected ions are accelerated along the shock normal at their re-crossing the shock. Their total pressure p_{xx} increases, which requires a compensatory decrease of the magnetic pressure. This contribution is opposite to the contribution of the directly transmitted ions and has a stabilizing effect. "Imagine now that the overshoot spontaneously grows a little. This would decrease the pressure of the directly transmitted ions and the ions which are being reflected. Without the reflected-transmitted ions this would cause further increase of the overshoot, as prescribed by the pressure balance. However, the increase of the overshoot would increase the number of reflected ions and, accordingly, the pressure of the reflected-transmitted ions. The latter increases from the beginning of the ramp through the overshoot, thus outplaying the decrease of the pressure of the directly transmitted ions across the same region and limiting the spontaneous overshoot growth. If the overshoot spontaneously decreases, the pressure of the directly-transmitted ions goes

up and the pressure of the reflected-transmitted ions goes down. Therefore, the reflected-transmitted ions play a stabilizing effect, ensuring that a balance could be achieved, where any spontaneous change of the overshoot strength would result in the corresponding change of the total pressure of all ion populations together in such a way to act against the spontaneous overshoot variation, thus making the shock structure stable. ”

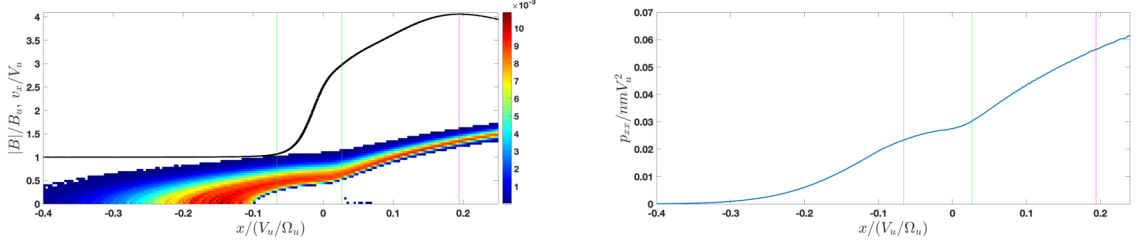


Figure 3: Left: reduced distribution function $f(x, v_x)$ of the reflected ions from their turning points up to the maximum of the overshoot. Right: their total pressure p_{xx} .

3.4 Relation of the ion distributions to the shock structure

Combining theory with the test particle analysis the relation between the Mach number, overshoot maximum, and cross-shock potential is established, and is further related to the downstream magnetic field (Gedalin, 2022).

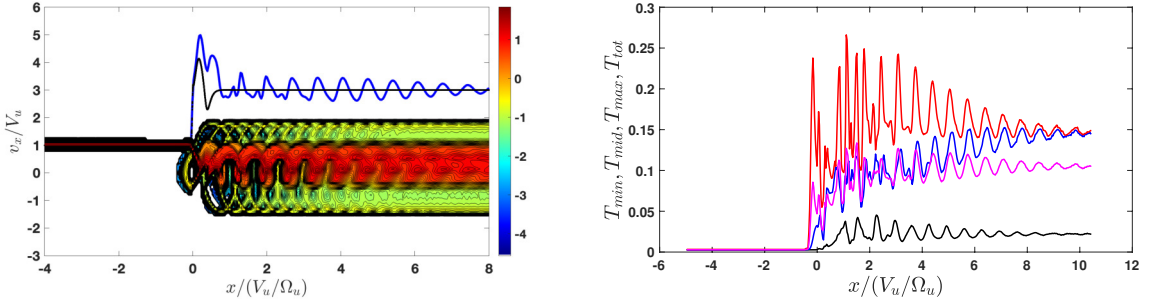


Figure 4: Left: The normalized model magnetic field (black curve), the magnetic field derived from the pressure balance (blue curve), and the reduced distribution function (log scale), for $M = 4.3$, $\theta = 60^\circ$, and $B_d/B_u = 3$, with overshoot and undershoot added. Right: Three eigenvalues of the temperature tensor and the total temperature (green).

The postshock non-gyrotropic distributions relax to gyrotropic-anisotropic distributions. Further relaxation to the isotropic shape may be slow. During this relaxation the magnetic field also changes (Gedalin et al., 2022).

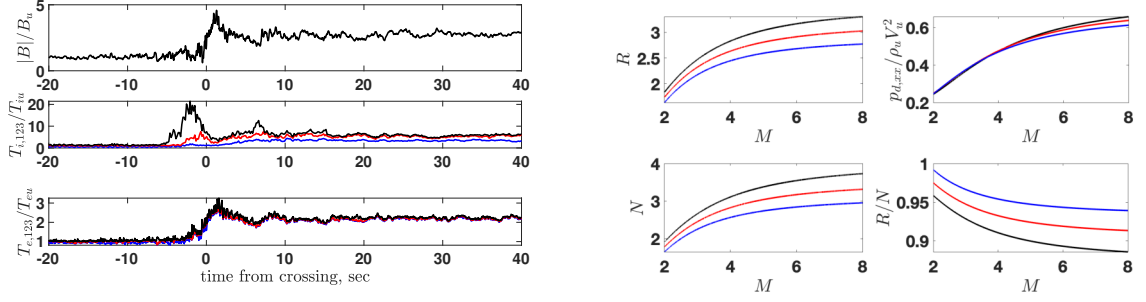


Figure 5: Left: Top: the magnetic field magnitude, normalized to the upstream magnetic field magnitude. Middle: the three eigenvalues of the ion temperature tensor, normalized to the upstream ion temperature. Bottom: the three eigenvalues of the electron temperature tensor, normalized on the upstream electron temperature. The smallest eigenvalue is in blue, the largest one is in black. The measurements are done in the burst mode. Right: Various parameters as functions of the Alfvénic Mach number M for $A = 1$ (black curves), $A = 0.5$ (red curves), and $A = 0.1$ (blue curves). Top left: the magnetic compression $R = B_d/B_u$. Top right: the normalized downstream pressure $\Pi_{xx} = p_{d,xx}/\rho_u V_u^2$. Bottom left: the density compression $N = n_d/n_u$. Bottom right: the ratio of the magnetic compression to the density compression R/N . The shock angle is $\theta_u = 60^\circ$ and $\beta = 0.5$.

3.5 An analytical model of rippling and implications

A first analytical model of the fields in a rippled shock front has been proposed (Gedalin & Ganushkina, 2022). Implications for upstream whistler wave-trains and postshock distributions have been analyzed. In addition, a gallery of patterns of the magnetic field, which would be observed by a single spacecraft, is produced. The internal document RipplingPatterns.pdf is attached.

3.6 Ion dynamics in non-rippled vs rippled shocks

Ion dynamics and distributions in rippled shocks have been analyzed with test particle analysis in quasi-perpendicular shocks (Gedalin et al., 2023b, submitted) and in an Solo Orbiter observed quasi-parallel shock (Dimmock et al., 2023, submitted).

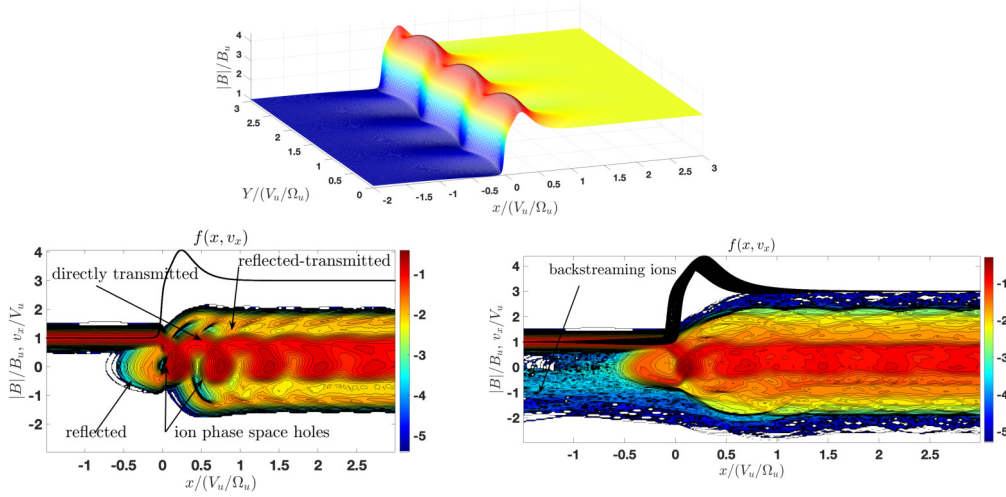


Figure 6: Top: The two-dimensional surface of the magnetic field magnitude for the rippled shock. Y is in the direction of rippling propagation. The global shock normal is along x . The local shock normal is determined by the steepest gradient of the magnetic field magnitude, depends on Y , and differs from the global normal. The maximum overshoot magnetic field also depends on Y . Bottom left: Reduced distribution function $f(x, v_x)$ for the case without rippling. The black line shows the magnetic field magnitude. All distinct ion populations are indicated on the top panel: a) the directly transmitted ions cross the shock and proceed further downstream, b) the reflected ions are seen just ahead of the shock transition, c) the reflected-transmitted ions are the reflected ions which cross the shock again and proceed further downstream. Ion phase space holes are the regions where the phase space density is very low and even approaches zero. Non-gyrotropy of the downstream distribution persists well into the downstream region. Bottom right: Reduced distribution function $f(x, v_x)$ for the case with rippling. The black ribbon shows the magnetic field magnitude as observed by ions crossing the shock in different positions. The directly transmitted, reflected, and reflected-transmitted ions are clearly seen but ion phase space holes are filled with ions. Gyrotropization of the downstream distribution occurs within one ion convective gyroradius. The most important change is the appearance of the backstreaming ions.

The test particle analysis of a quasi-perpendicular shock (Gedalin et al., 2023b) revealed that rippling may produce backstreaming ions which are not present in a planar shock.

Observations of an oblique, marginally quasi-parallel, θ_{Bn} , shock (Dimmock et al., 2023, submitted) have found backstreaming ions.

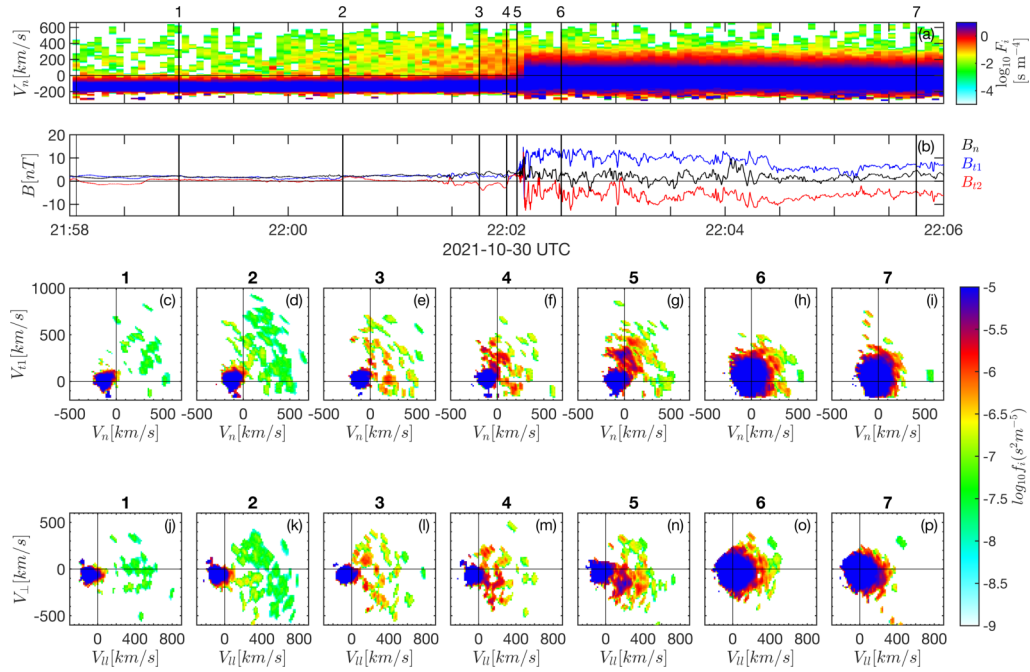


Fig. 6. Evolution of ion VDFs across the shock. Panel (a) shows a reduced distribution of phase space density along the shock normal whereas plotted in panel (b) is the magnetic field in shock coordinates. The bottom panels are ion VDFs in the $\hat{n} - \hat{t}_1$ plane (c-i) and $\hat{B}_{\parallel} - \hat{B}_{\perp}$, at various locations from upstream to downstream of the shock front. Note that \hat{B}_{\parallel} refers to \mathbf{B}_u . Noticeable is an ion population (in all the VDFs) separate from the solar wind beam.

Further test particle analysis have shown that in this case there is little difference between rippled and non-rippled profiles.

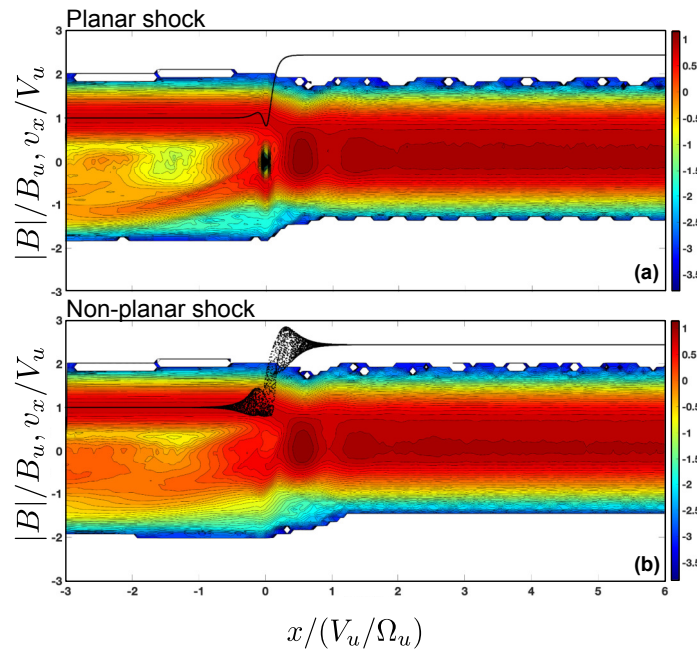


Fig. 9. Both panels show test particle analysis for a shock with equivalent parameters to the one observed by SolO. The difference between panels (a) and (b) are that the analysis was performed for a planar and non-planar shock, respectively.

The backstreaming ion distribution is more diffuse for a rippled shock, and the number of these particles is a little larger.

3.7 Nonlocal reflection

Reflected ions move along the shock front, and the distance between the reflection point and the re-entry point. Until now only the shift in the direction perpendicular to the coplanarity plane was of interest, since it is related to the foot formation. However, the distance and the direction of the shift depend on the shock angle (Gedalin, 2023, submitted). This nonlocality of the ion reflection

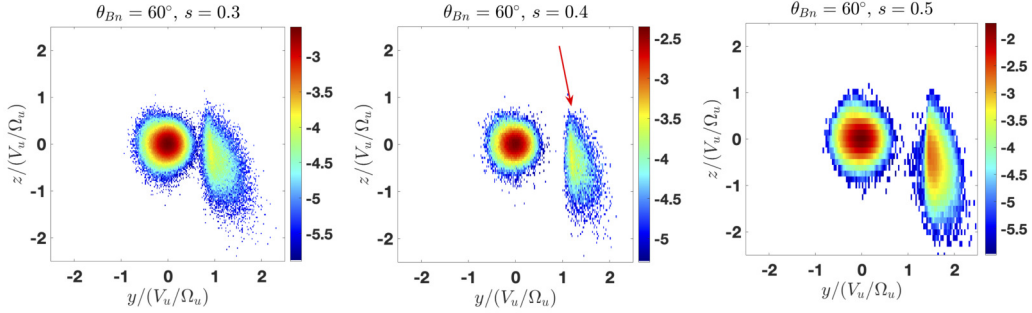


Figure 7: y and z -coordinates of the ions crossing the red line position for $\theta_{Bn} = 60^\circ$ and three different values of $s = 0.3, 0.4, 0.5$. The value of the cross-shock potential affects the dispersion of the positions but only weakly affects the position of the maximum.

may be related to the rippling development since the reflected ions can carry perturbations along the shock front. The estimated wavelength and speed of the ripples are consistent with those found earlier in simulations (Burgess et al., 2026).

4 References

- M. Balikhin and M. Gedalin. Collisionless Shocks in the Heliosphere: Foot Width Revisited. *Astrophys. J.*, 925, 90, J 2022. doi: [10.3847/1538-4357/ac3bb3](https://doi.org/10.3847/1538-4357/ac3bb3).
- D. Burgess, D., P. Hellinger, I. Gingell, & P. M. Trávníček. Microstructure in two- and three-dimensional hybrid simulations of perpendicular collisionless shocks. *J. Plasma Phys.*, 82, 905820401, 2016.
- A. P. Dimmock, M. Gedalin, A. Lalti, 3, D. Trotta, Yu. V. Khotyaintsev, D. B. Graham, A. Johlander, 1, R. Vainio, X. Blanco-Cano, P. Kajdic, C. J. Owen, and R. F. Wimmer-Schweingruber, Backstreaming ions at a high Mach number oblique interplanetary shock, Solar Orbiter measurements during the main phase, *Astron. Astrophys.*, 2023, (submitted).
- M. Gedalin. Combining Rankine–Hugoniot relations, ion dynamics in the shock front, and the cross-shock potential. *Phys. Plasmas*, 29, 112904, 2022. doi: [10.1063/5.0120578](https://doi.org/10.1063/5.0120578).
- M. Gedalin, M. Golan, N. V. Pogorelov, and V. Roytershteyn. Change of Rankine–Hugoniot Relations during Postshock Relaxation of Anisotropic Distributions. *Astrophys. J.*, 940, 21, 2022. doi: [10.3847/1538-4357/ac958d](https://doi.org/10.3847/1538-4357/ac958d).
- M. Gedalin and N. Ganushkina. Implications of weak rippling of the shock ramp on the pattern of the electromagnetic field and ion distributions. *J. Plasma Phys.*, 88, 905880301, 2022. doi: [10.1017/S0022377822000356](https://doi.org/10.1017/S0022377822000356).
- M. Gedalin, A. P. Dimmock, C. T. Russell, N. V. Pogorelov, and V. Roytershteyn. Role of the overshoot in the shock self-organization. *J. Plasma Phys.*, 89, 905890201, 2023a. doi: [10.1017/S0022377823000090](https://doi.org/10.1017/S0022377823000090).
- M. Gedalin, N. V. Pogorelov, and V. Roytershteyn, Scattering of ions at a rippled shock, *Astrophys. J.*, 2023b. (accepted).
- M. Gedalin, Non-locality of ion reflection at the shock front: Dependence on the shock angle, *J. Plasma Phys.*, 2023 (submitted).
- M. Gedalin and P. Sharma, Effect of the reflected ions on the magnetic overshoot of a collisionless shock, *Phys. Plas.* 2023 (submitted)
- Gosling, J. T., & Thomsen, M. F. *J. Geophys. Res.*, 90, 9893, 1985. doi: [10.1029/JA090iA10p09893](https://doi.org/10.1029/JA090iA10p09893)
- P. Sharma and M. Gedalin, Non-specular ion reflection at quasiperpendicular collisionless shock front, *J. Plasma Phys.*, 2023 (submitted).